



On the Origin of High-energy Neutrinos from NGC 1068: The Role of Nonthermal Coronal Activity

Yoshiyuki Inoue^{1,2} , Dmitry Khangulyan³ , and Akihiro Doi^{4,5} ¹ Interdisciplinary Theoretical & Mathematical Science Program (iTHEMS), RIKEN, 2-1 Hirosawa, Saitama 351-0198, Japan; yoshiyuki.inoue@riken.jp² Kavli Institute for the Physics and Mathematics of the Universe (WPI), UTIAS, The University of Tokyo, Kashiwa, Chiba 277-8583, Japan³ Department of Physics, Rikkyo University, Nishi-Ikebukuro 3-34-1, Toshima-ku, Tokyo 171-8501, Japan; d.khangulyan@rikkyo.ac.jp⁴ Institute of Space and Astronautical Science JAXA, 3-1-1 Yoshinodai, Chuo-ku, Sagamihara, Kanagawa 252-5210, Japan; akihiro.doi@vsop.isas.jaxa.jp⁵ Department of Space and Astronautical Science, The Graduate University for Advanced Studies (SOKENDAI), 3-1-1 Yoshinodai, Chuo-ku, Sagamihara, Kanagawa 252-5210, Japan

Received 2020 January 21; revised 2020 February 13; accepted 2020 February 13; published 2020 March 9

Abstract

NGC 1068, a nearby type-2 Seyfert galaxy, is reported as the hottest neutrino spot in the 10 yr survey data of IceCube. Although there are several different possibilities for the generation of high-energy neutrinos in astrophysical sources, feasible scenarios allowing such emission in NGC 1068 have not yet been firmly defined. We show that the flux level of GeV and neutrino emission observed from NGC 1068 implies that the neutrino emission can be produced only in the vicinity of the supermassive black hole in the center of the galaxy. The coronal parameters, such as magnetic field strength and corona size, that make this emission possible, are consistent with the spectral excess registered in the millimeter range. The suggested model and relevant physical parameters are similar to those revealed for several nearby Seyferts. Due to the internal gamma-ray attenuation, the suggested scenario cannot be verified by observations of NGC 1068 in the GeV and TeV gamma-ray energy bands. However, the optical depth is expected to become negligible for MeV gamma-rays, thus future observations in this band will be able to validate our model.

Unified Astronomy Thesaurus concepts: Astrophysical black holes (98); Black hole physics (159); Black holes (162); Supermassive black holes (1663); Neutrino astronomy (1100); Active galactic nuclei (16); Seyfert galaxies (1447); Particle astrophysics (96); High energy astrophysics (739); Accretion (14)

1. Introduction

IceCube registered the first astrophysical neutrinos with energies of TeV–PeV several years ago (Aartsen et al. 2013). However, their origin remains uncertain. Recently, a nearby Seyfert galaxy NGC 1068, which appeared as the hottest spot in all-sky 10 yr survey data of IceCube, was reported to be a neutrino source with a 2.9σ confidence level (Aartsen et al. 2020). Thus, studying possible neutrino production mechanisms in NGC 1068 is a timely task that may provide a key clue for unveiling the origin of the cosmic diffuse neutrino background flux.

Production of very-high-energy (VHE) neutrinos is accompanied by emission of gamma-rays and the luminosity of that component exceeds the neutrino one. NGC 1068 is known as a gamma-ray emitter (Lenain et al. 2010; Ajello et al. 2017; The Fermi-LAT Collaboration 2019). However, the reported neutrino flux is higher than the GeV gamma-ray flux (Aartsen et al. 2020). Thus, it requires a significant attenuation of GeV gamma-rays. Unless one adopts a very exotic spectrum of emitting particles, this implies the presence of enough dense X-ray target photons, $\epsilon_X \sim 1$ keV. The gamma-ray optical depth τ depends on the X-ray luminosity of this component L_X and the size of the production regions R :

$$\tau \approx \frac{\sigma_T}{4\pi c} \epsilon_X^{-1} L_X R^{-1} \simeq 10^5 \left(\frac{\epsilon_X}{1 \text{ keV}} \right)^{-1} \frac{L_X}{L_{\text{Edd}}} \frac{R_s}{R}, \quad (1)$$

where L_{Edd} is the Eddington luminosity and R_s is the Schwarzschild radius. Although this estimate is not sensitive to the mass of the source, it suggests that such a dense X-ray target can exist only in the vicinity of compact objects.

A large number, $\mathcal{N} \sim 10^3$, of stellar-mass black hole (or neutron star) systems, i.e., X-ray binaries, can produce neutrinos with the flux level required by the IceCube detection without violating the above criteria. Their typical luminosity distribution in a galaxy is represented by a power law as $dN/dL_X \propto L_X^{-1.6}$ (Swartz et al. 2011). This implies that the dominant contributor is the higher-luminosity systems. However, NGC 1068 hosts only three X-ray binaries with $L_X \geq 10^{39}$ erg s⁻¹ (Swartz et al. 2011), thus their number is not sufficient at least by several orders of magnitude. The only remaining candidate is the supermassive black holes (SMBHs) at the center of the galaxy. The high accretion rate, implied by the intrinsic X-ray luminosity of $L_X \sim 10^{-2} L_{\text{Edd}}$ (Bauer et al. 2015; Marinucci et al. 2016), does not allow an effective particle acceleration in the central black hole magnetosphere. Thus, emission of VHE neutrinos from the vicinity of SMBHs indicates the operation of efficient nonthermal particle acceleration in the active galactic nuclei (AGNs) coronae.

NGC 1068 is a type-2 Seyfert galaxy, which is a class of AGN, emitting intense electromagnetic radiation in a broad range of frequencies. The intrinsic X-ray emission is generated through Comptonization of accretion-disk photons in hot plasma above the disk, namely in coronae (e.g., Katz 1976; Bisnovatyi-Kogan & Blinnikov 1977; Pozdniakov et al. 1977; Galeev et al. 1979; Takahara 1979). The typical size of the AGN corona is about $\gtrsim 10 R_s$. If high-energy particles are accelerated in the corona, the nucleus of NGC 1068 is a plausible candidate for the observed neutrinos, which is consistent with a number of previous studies (see e.g., Begelman et al. 1990; Stecker et al. 1992; Kalashev et al. 2015; Inoue et al. 2019; Murase et al. 2019). There has been no

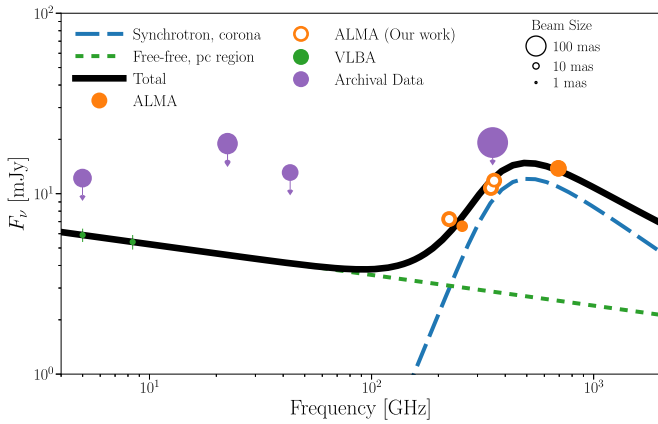


Figure 1. Centimeter–millimeter spectrum of NGC 1068. The data points from VLBA (Gallimore et al. 2004) and ALMA (García-Burillo et al. 2016, 2019; Impellizzeri et al. 2019) are shown in green and orange, respectively. The open points represent the newly analyzed ALMA data. The size of circles corresponds to the beam sizes, as indicated in the figure. We also show the archival millimeter–centimeter data with large beam sizes as upper limits in purple (Gallimore et al. 1996; Cotton et al. 2008; Pasetto et al. 2019). The error bars correspond to 1σ uncertainties, although those cannot be clearly seen because of their small errors. The blue-dashed and green-dotted lines show the coronal synchrotron and parsec-scale free–free components, respectively. The black solid line shows the sum of these two components.

clear observational evidence for the nonthermal coronal activity (Lin et al. 1993; Madejski et al. 1995). However, as several corona parameters, e.g., magnetic field strength and corona size, remain highly uncertain, one cannot rule out the presence of high-energy particles in AGN coronae. These parameters have a critical impact on the expected nonthermal flux level.

The coronal synchrotron emission is key for dissolving this problem, as it reflects the nonthermal coronal activity directly and allows determination of corona magnetic properties (e.g., Di Matteo et al. 1997; Inoue & Doi 2014). By combining the radio and X-ray spectra, one can also determine the size of coronae. A characteristic feature of the coronal synchrotron emission is a spectral excess in the millimeter band, so-called millimeter excess. However, previous observations presented inconclusive evidence of such excess in the radio spectra of several Seyfert galaxies. A key observational challenge in registering the excess is the contamination by extended galactic emission and a paucity of multi-band data (Antonucci & Barvainis 1988; Barvainis et al. 1996; Doi & Inoue 2016; Behar et al. 2018).

Recently, Inoue & Doi (2018) reported the detection of nonthermal coronal radio synchrotron emission from two nearby Seyferts, IC 4329A and NGC 985, utilizing the Atacama Large Millimeter/submillimeter Array (ALMA), which enabled multi-band observations with high enough angular resolution to exclude the galactic contamination. These observations provided the first determination of the key physical parameters of the corona: magnetic field strength and its size. Given the coronal parameters constrained by X-ray and radio observations, the nonthermal acceleration process there should be capable of boosting particle energy to the very-high-energy band, resulting in the generation of high-energy gamma-ray and neutrino emission (Inoue et al. 2019).

Very Long Baseline Array (VLBA) radio observations detected a homogeneous emission at the centimeter bands from the central parsec of NGC 1068. The reported flux is attributed to the free–free emission (Gallimore et al. 2004).

This spectrum is not consistent with the fluxes observed at higher frequencies and millimeter bands, which show a spectral excess (see the Section 2). Because of the spectral shape the excess component should be produced by nonthermal particles localized in a much more compact region with a size similar to that of the corona.

In this Letter, we study the constraints on the nonthermal particles in the corona of NGC 1068 imposed by the observations in the radio and gamma-ray bands. We check if the reported flux of VHE neutrino is consistent with the revealed properties of the corona nonthermal particles. We also discuss the reason why NGC 1068 appears as the hottest spot among other Seyfert galaxies based on the corona scenario.

2. Observational Properties

NGC 1068 is one of the nearest and best-studied Seyfert 2 galaxies in the broad band (see, e.g., Pasetto et al. 2019, for details), where the central engine is supposed to be blocked by the dusty torus. It is located at a distance of ~ 14 Mpc ($1'' \sim 70$ pc, Tully 1988).

The mass of the central black hole is still uncertain. It is estimated as $\sim 1 \times 10^7 M_\odot$ from the measurement of the rotational motion of a water maser disk (Greenhill et al. 1996; Huré 2002; Lodato & Bertin 2003). However, the rotation curve is non-Keplerian (Lodato & Bertin 2003). The SMBH mass is also estimated as $\sim 7 \times 10^7 M_\odot$ and $\sim 1 \times 10^8 M_\odot$ from the polarized broad Balmer emission line and the neutral FeK α line, respectively (Minezaki & Matsushita 2015). In this study, we adopt $5 \times 10^7 M_\odot$ as the mass of the central SMBH of NGC 1068.

In centimeter radio observations, the jets are prominent and extend for several kiloparsecs in both directions. In the central $\sim 1''$ region, the downstream jet emission dominates in the centimeter regime. The jet changes its direction at $\sim 0''.2$ away from the nuclear region. This change is presumed to be the result of an interaction with a molecular cloud (Gallimore et al. 1996, 2004; Cotton et al. 2008). At long wavelengths, the VLBA 1.4, 5, and 8.4 GHz (centimeter bands) observations reported the flux of 5.9 ± 0.5 mJy with a spectral index of -0.17 above 5 GHz and nondetection at 1.4 GHz, indicating strong attenuation below 5 GHz (Gallimore et al. 2004). At 5 GHz, the brightness temperature is $\sim 2.5 \times 10^6$ K, which is too low for synchrotron self-absorption flux unless the magnetic fields are order of 10^9 G (Gallimore et al. 1996, 2004). As discussed in Gallimore et al. (2004), the free–free emission is the most likely origin of the 5 and 8.4 GHz flux. The emission-region size is ~ 0.8 pc, with a temperature of $\sim 10^6$ K and the electron density of $\sim 8 \times 10^5 \text{ cm}^{-3}$, which is irrelevant to the central corona and much more extended. At short wavelengths (millimeter bands), the central compact region starts to dominate the entire emission (Cotton et al. 2008; Imanishi et al. 2018). Together with multi-frequency observations, a possible spectral excess was reported in the nucleus component (Krips et al. 2006; Pasetto et al. 2019). Recently, high angular resolution observations with ALMA detected 6.6 ± 0.3 mJy and 13.8 ± 1.0 mJy flux from the core at 256 GHz and 694 GHz, respectively (García-Burillo et al. 2016; Impellizzeri et al. 2019). As the expected free–free component at the millimeter band based on the VLBA observations is only at ~ 4 mJy, a new spectral component is emerging in the millimeter band.

In X-rays, NGC 1068 was first studied by *Ginga* (Koyama et al. 1989), where intense iron line was reported together with an estimate for the intrinsic X-ray luminosity of 10^{43-44} erg s $^{-1}$. Later, it is reported that the observed X-ray emission is due to the reflected component (e.g., Ueno et al. 1994). Utilizing *NuSTAR* and other existing X-ray observatories, the reflected emission is revealed to have originated in multiple reflection components (Bauer et al. 2015; Marinucci et al. 2016). The intrinsic 2–10 keV luminosity is estimated as $L_X = 7_{-4}^{+7} \times 10^{43}$ erg s $^{-1}$ (Marinucci et al. 2016), while according to Bauer et al. (2015) it is 2.2×10^{43} erg s $^{-1}$. In this Letter, we take the value of $L_X = 7 \times 10^{43}$ erg s $^{-1}$ as the fiducial value.

3. Coronal Synchrotron Emission

Figure 1 shows the centimeter–millimeter spectrum of NGC 1068 based on measurements reported by Gallimore et al. (2004), García-Burillo et al. (2016), and Impellizzeri et al. (2019), where the beam size is ~ 2 , ~ 50 , ~ 20 mas, respectively. In addition, we obtain the continuum fluxes at 224, 345, and 356 GHz with beam sizes of 30 mas by analyzing the latest ALMA band 6 and 7 data (2016.1.00232.S, García-Burillo et al. 2019). We also show the archival core region data sets with beam sizes >50 mas as upper limits (Gallimore et al. 1996; Cotton et al. 2008; Pasetto et al. 2019).

NGC 1068 shows a millimeter excess similar to those observed in previous objects (Inoue & Doi 2018). However, we cannot claim a firm detection of this component in NGC 1068, because of a paucity of flux measurements, mixture of beam sizes, and the complex source structure. In this Letter, motivated by the possible neutrino detection (Aartsen et al. 2020) and detection of coronal synchrotron emission in other Seyferts (Inoue & Doi 2018), we consider specifically the possibility of coronal synchrotron emission to explain this millimeter excess. The coronal synchrotron self-absorption, breaking the spectrum between 300 and 600 GHz, would imply a firm relation between the corona magnetic field and size, putting constraints on the acceleration process at work in the corona.

The excess of NGC 1068 can be reproduced with the coronal synchrotron emission model with parameters of the corona size $R_c = 10 R_s$, the magnetic field strength $B = 100$ G, and the spectral index of nonthermal electrons $p = 2.7$ on top of free-free emission produced in parsec-size region (Gallimore et al. 2004). A much softer spectral index would violate either the ALMA measurements or the flux upper limit at 351 GHz (Figure 1). The required coronal size is consistent with optical–X-ray spectral fitting studies (Jin et al. 2012) and microlensing observation (Morgan et al. 2012) in other Seyferts. The previously reported coronal synchrotron objects IC 4329A and NGC 985, whose black hole masses are $\sim 10^8 M_\odot$, have $R_c \sim 40 R_s$ and $B \sim 10$ G (Inoue & Doi 2018), which are similar to what we required for the excess in NGC 1068 for the coronal synchrotron emission scenario.

Although we chose the coronal synchrotron emission model as a possible explanation for the millimeter excess, current data sets do not allow us to provide clear evidence. Future ALMA observations will be able to elucidate the origin of the excess. High angular resolution observations will be able to precisely understand the contribution of the free–free component. Multi-frequency and variability measurements in the millimeter band

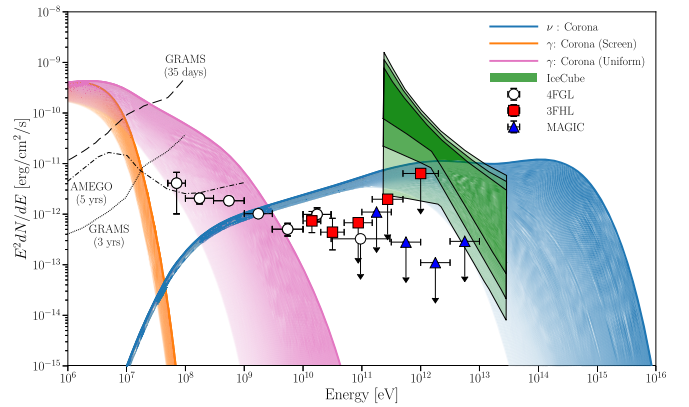


Figure 2. Gamma-ray and neutrino spectrum of NGC 1068. The circle, square, and triangle data points are from The Fermi-LAT Collaboration (2019), Ajello et al. (2017), and Acciari et al. (2019), respectively. The green shaded regions represent the 1σ , 2σ , and 3σ regions on the spectrum measured by IceCube (Aartsen et al. 2020). The expected gamma-ray and neutrino spectrum from the corona are shown for $30 \leq \eta_g \leq 3 \times 10^4$. The darker region corresponds to lower η_g . The blue region shows the expected neutrino spectrum. The orange and magenta shaded region shows the gamma-ray spectrum for the uniform case and the screened case, respectively. We also overplot the sensitivity curves of GRAMS (Aramaki et al. 2020) and AMEGO (McEnery et al. 2019) for comparison.

will be also able to determine the spectral shape and see the coronal activity.

The coronal synchrotron emission is mostly determined by the following parameters: R_c , B , p , and the energy fraction of nonthermal electrons (f_{nth}). We fix the energy fraction of nonthermal electrons as $f_{\text{nth}} = 0.03$, which is required to explain the cosmic MeV gamma-ray background radiation by the Comptonization counterpart (Inoue et al. 2019). We adopt standard coronal temperature and Thomson scattering optical depth value of 100 keV and 1.1, respectively (Inoue et al. 2019), because both of them are not determined in Marinucci et al. (2016).

4. Coronal Gamma-Ray and Neutrino Emission

We investigate the properties of high-energy emission from the nucleus of NGC 1068 utilizing the derived coronal parameters based on the possible millimeter excess (see Figure 1). Observations of the electromagnetic emission constrain the parameters of the gamma-ray and neutrino production model (Inoue et al. 2019), except for the energy injection ratio between protons and electrons and the gyrofactor η_g , which is the mean-free path of a particle in units of gyroradius.

Particles are expected to be accelerated by the diffusive shock acceleration. Other mechanisms such as magnetosphere, turbulence, or reconnection cannot explain the required electron distribution for the coronal synchrotron emission because of a high accretion rate and low magnetic field strength (See Section 8.3 in Inoue et al. 2019 for details). Gamma-rays are generated through the Comptonization of disk photons and/or hadronic interactions in coroneae. Hadronic interactions generate neutrinos. Because of the intense X-ray and UV photon field from the corona and the accretion disk, $\gtrsim 100$ MeV gamma-rays are significantly attenuated.

Figure 2 shows the expected gamma-ray and neutrino signals from NGC 1068 together with the observed gamma-ray data (Ajello et al. 2017; Acciari et al. 2019; The Fermi-LAT Collaboration 2019) and the IceCube data (Aartsen et al.

2020). The data is taken from Figure 7 of Aartsen et al. (2020), and the 1σ , 2σ , and 3σ regions are shown in the plot. For the comparison, we also show the expected sensitivity curves of a future MeV gamma-ray mission, *GRAMS* (Aramaki et al. 2020), and *AMEGO* (McEnery et al. 2019). Gamma-ray model curve is the summation of leptonic and hadronic gamma-rays after internal (X-ray corona and UV accretion-disk photons) and intergalactic (on EBL photons) attenuation. For hadronic processes, we consider both pp and $p\gamma$ interactions.

We follow the same assumptions for the coronal parameters used in Inoue et al. (2019), except for the gyrofactor and parameters determined by the coronal synchrotron model explaining the millimeter excess. Considering the measurement uncertainty, in the figure, we plot the model curve region in the range of $30 \leq \eta_g \leq 3 \times 10^4$ for each curve. The darker region corresponds to lower η_g , in which models extend to higher energies. The injection powers in protons and electrons are set to equal, as assumed in Inoue et al. (2019).

The gyrofactor $\eta_g = 30$ was required in order to explain the measured TeV diffuse neutrinos (Inoue et al. 2019). We note that the model curve with this η_g is still acceptable, given the measurement uncertainty (according to the Figure 4 of Aartsen et al. 2020, the neutrino spectral index is constrained to a broad range above 2). A more detailed neutrino spectrum will allow us to narrow down the range of η_g . If future data require $\eta_g \gg 30$, it will suggest that Seyferts are sub-dominant contributors to the diffuse neutrino background fluxes.

As NGC 1068 is an AGN, it also features a bright accretion disk and a hot corona. The disk and corona emission absorb gamma-rays via pair creation. For the internal gamma-ray attenuation, we consider two cases. One is the “uniform” emissivity case as assumed in Inoue et al. (2019), while the other is the “screened” case. In the uniform emissivity case, gamma-rays and target photons are uniformly distributed. Gamma-rays are attenuated by a factor of $3u(\tau)/\tau$, where $u(\tau) = 1/2 + \exp(-\tau)/\tau - [1 - \exp(-\tau)]/\tau^2$. Here τ is the gamma-ray optical depth computed from the center of the corona. In the screened case, gamma-rays are assumed to be generated in the inner part of the corona, and the dominant attenuating photon field surrounds it. Since the disk and corona temperature depend on the disk radius (Kawanaka et al. 2008), this configuration is possible. Then, gamma-rays are attenuated by a factor of $\exp(-\tau)$. Gamma-rays are also attenuated by the intergalactic photons during the propagation to the Earth. In this Letter, we adopt Inoue et al. (2013) for the intergalactic attenuation.

In the screened case, the model can explain the preliminary neutrino signals above several TeV without violating the gamma-ray data. On the other hand, the uniform emissivity model violates the low-energy gamma-ray data. This implies a more detailed study of the coronal geometry is necessary. Future MeV gamma-ray missions such as *GRAMS* (Aramaki et al. 2020) and *AMEGO* (McEnery et al. 2019) will verify our model and help us to understand the coronal geometry, which is not yet well understood.

Due to the internal attenuation, it is not easy for the corona model to explain the entire observed gamma-ray flux data up to 20 GeV, requiring another mechanism to explain gamma-rays above 100 MeV, such as star formation activity (Ackermann et al. 2012), jet (Lenain et al. 2010), or disk wind (Lamastra et al. 2016).

5. Discussions and Conclusion

The IceCube Collaboration reported NGC 1068 as the hottest spot in their 10 yr survey (Aartsen et al. 2020). Surprisingly, the reported neutrino flux is higher than the GeV gamma-ray flux, which requires different origins and a significant attenuation of GeV gamma-rays from the neutrino production site. This further implies a presence of enough dense X-ray target photons in the neutrino production region in order to attenuate gamma-rays $\gtrsim 100$ MeV. Such a dense X-ray target can exist only in the vicinity of compact objects. However, stellar-mass objects such as X-ray binaries cannot explain the whole neutrino flux because the number of such objects in NGC 1068 is several orders of magnitude lower than is required. The only feasible candidate is the coronal activity of SMBHs at the center of the galaxy.

NGC 1068 is one of the best-studied type-2 Seyfert galaxies. The nucleus flux in the centimeter band comes from the free-free emission component (Gallimore et al. 2004). However, at higher frequencies, an excess of core flux is reported utilizing ALMA (García-Burillo et al. 2016; Impellizzeri et al. 2019). We found that the coronal synchrotron emission model can reproduce the observed millimeter spectrum, which puts constraints on the acceleration process in the corona.

Given the corona parameters revealed with ALMA measurements, we studied the resulting gamma-ray and neutrino emissions from the corona of NGC 1068. Although it is difficult to explain the gamma-ray flux above 100 MeV due to significant internal attenuation effects, the coronal emission can explain the reported IceCube neutrino flux with a gyrofactor in the range of $30 \leq \eta_g \leq 3 \times 10^4$. Further neutrino data on NGC 1068 will narrow down the required range of η_g . It should be noted that $\eta_g \sim 30$ is required for Seyferts to explain the diffuse neutrino fluxes up to 300 TeV (Inoue et al. 2019).

In order to not violate the observed gamma-ray data, the corona cannot be uniform. The dominant attenuating photon field needs to surround the gamma-ray emission region. Since the disk temperature depends on the disk radius, such a configuration can be realized. Future MeV gamma-ray observations will be a critical tool to test the corona scenario.

An important question is what differs NGC 1068 from other nearby Seyfert galaxies. NGC 1068 is not the brightest X-ray Seyfert (Oh et al. 2018). Its observed hard X-ray flux is a factor of ~ 16 fainter than that of the brightest Seyfert, NGC 4151. NGC 1068 is a type-2 Seyfert galaxy, and is obscured by the materials up to the neutral hydrogen column density of $N_H \sim 10^{25} \text{ cm}^{-2}$ (Bauer et al. 2015; Marinucci et al. 2016). If we correct this attenuation effect to understand the intrinsic X-ray radiation power, NGC 1068 appears to be the intrinsically brightest Seyfert. For example, intrinsically, it would be by a factor of ~ 3.6 brighter than NGC 4151 in X-rays. As the dusty torus does not obscure coronal neutrino emission, which can scale with accretion power, NGC 1068 might be the brightest source of VHE neutrinos. This could be the reason why NGC 1068 appears to be the hottest spot in the IceCube map rather than other Seyfert galaxies.

The authors thank the anonymous referee for thoughtful and helpful comments. Y.I. is supported by JSPS KAKENHI grants No. JP16K13813, JP18H05458, and JP19K14772; the program of Leading Initiative for Excellent Young Researchers, MEXT, Japan; and the RIKEN iTHEMS Program. D.K. is supported by JSPS KAKENHI grants No. JP18H03722, JP24105007, and

JP16H02170. This paper makes use of the following ALMA data: ADS/JAO.ALMA#2016.1.00232.S. ALMA is a partnership of ESO (representing its member states), NSF (USA) and NINS (Japan), together with NRC (Canada), *MOST* and ASIAA (Taiwan), and KASI (Republic of Korea), in cooperation with the Republic of Chile. The Joint ALMA Observatory is operated by ESO, AUI/NRAO, and NAOJ.

ORCID iDs

Yoshiyuki Inoue  <https://orcid.org/0000-0002-7272-1136>

Dmitry Khangulyan  <https://orcid.org/0000-0002-7576-7869>

Akihiro Doi  <https://orcid.org/0000-0003-4384-9568>

References

- Aartsen, M. G., Abbasi, R., Abdou, Y., et al. 2013, *PhRvL*, **111**, 021103
- Aartsen, M. G., Ackermann, M., Adams, J., et al. 2020, *PhRvL*, **124**, 051103
- Acciari, V. A., Ansoldi, S., Antonelli, L. A., et al. 2019, *ApJ*, **883**, 135
- Ackermann, M., Ajello, M., Allafort, A., et al. 2012, *ApJ*, **755**, 164
- Ajello, M., Atwood, W. B., Baldini, L., et al. 2017, *ApJS*, **232**, 18
- Antonucci, R., & Barvainis, R. 1988, *ApJL*, **332**, L13
- Aramaki, T., Hansson Adrian, P., Karagiorgi, G., & Odaka, H. 2020, *Aph*, **114**, 107
- Barvainis, R., Lonsdale, C., & Antonucci, R. 1996, *AJ*, **111**, 1431
- Bauer, F. E., Arévalo, P., Walton, D. J., et al. 2015, *ApJ*, **812**, 116
- Begelman, M. C., Rudak, B., & Sikora, M. 1990, *ApJ*, **362**, 38
- Behar, E., Vogel, S., Baldi, R. D., Smith, K. L., & Mushotzky, R. F. 2018, *MNRAS*, **478**, 399
- Bisnovatyi-Kogan, G. S., & Blinnikov, S. I. 1977, *A&A*, **59**, 111
- Cotton, W. D., Jaffe, W., Perrin, G., & Woillez, J. 2008, *A&A*, **477**, 517
- Di Matteo, T., Celotti, A., & Fabian, A. C. 1997, *MNRAS*, **291**, 805
- Doi, A., & Inoue, Y. 2016, *PASJ*, **68**, 56
- Galeev, A. A., Rosner, R., & Vaiana, G. S. 1979, *ApJ*, **229**, 318
- Gallimore, J. F., Baum, S. A., & O'Dea, C. P. 2004, *ApJ*, **613**, 794
- Gallimore, J. F., Baum, S. A., O'Dea, C. P., & Pedlar, A. 1996, *ApJ*, **458**, 136
- García-Burillo, S., Combes, F., Ramos Almeida, C., et al. 2016, *ApJL*, **823**, L12
- García-Burillo, S., Combes, F., Ramos Almeida, C., et al. 2019, *A&A*, **632**, A61
- Greenhill, L. J., Gwinn, C. R., Antonucci, R., & Barvainis, R. 1996, *ApJL*, **472**, L21
- Huré, J. M. 2002, *A&A*, **395**, L21
- Imanishi, M., Nakanishi, K., Izumi, T., & Wada, K. 2018, *ApJL*, **853**, L25
- Impellizzeri, C. M. V., Gallimore, J. F., Baum, S. A., et al. 2019, arXiv:1908.07981
- Inoue, Y., & Doi, A. 2014, *PASJ*, **66**, L8
- Inoue, Y., & Doi, A. 2018, *ApJ*, **869**, 114
- Inoue, Y., Inoue, S., Kobayashi, M. A. R., et al. 2013, *ApJ*, **768**, 197
- Inoue, Y., Khangulyan, D., Inoue, S., & Doi, A. 2019, *ApJ*, **880**, 40
- Jin, C., Ward, M., Done, C., & Gelbord, J. 2012, *MNRAS*, **420**, 1825
- Kalashov, O., Semikoz, D., & Tkachev, I. 2015, *JETP*, **120**, 541
- Katz, J. I. 1976, *ApJ*, **206**, 910
- Kawanaka, N., Kato, Y., & Mineshige, S. 2008, *PASJ*, **60**, 399
- Koyama, K., Inoue, H., Tanaka, Y., et al. 1989, *PASJ*, **41**, 731
- Kripi, M., Eckart, A., Neri, R., et al. 2006, *A&A*, **446**, 113
- Lamastra, A., Fiore, F., Guetta, D., et al. 2016, *A&A*, **596**, A68
- Lenain, J. P., Ricci, C., Türler, M., Dorner, D., & Walter, R. 2010, *A&A*, **524**, A72
- Lin, Y. C., Bertsch, D. L., Dingus, B. L., et al. 1993, *ApJL*, **416**, L53
- Lodato, G., & Bertin, G. 2003, *A&A*, **398**, 517
- Madejski, G. M., Zdziarski, A. A., Turner, T. J., et al. 1995, *ApJ*, **438**, 672
- Marinucci, A., Bianchi, S., Matt, G., et al. 2016, *MNRAS*, **456**, L94
- McEnery, J., van der Horst, A., Dominguez, A., et al. 2019, *BAAS*, **51**, 245
- Minezaki, T., & Matsushita, K. 2015, *ApJ*, **802**, 98
- Morgan, C. W., Hainline, L. J., Chen, B., et al. 2012, *ApJ*, **756**, 52
- Murase, K., Kimura, S. S., & Meszaros, P. 2019, arXiv:1904.04226
- Oh, K., Koss, M., Markwardt, C. B., et al. 2018, *ApJS*, **235**, 4
- Pasetto, A., González-Martín, O., Esparza-Arredondo, D., et al. 2019, *ApJ*, **872**, 69
- Pozdniakov, L. A., Sobol, I. M., & Siuniaev, R. A. 1977, *SvA*, **21**, 708
- Stecker, F. W., Done, C., Salamon, M. H., & Sommers, P. 1992, *PhRvL*, **69**, 2738
- Swartz, D. A., Soria, R., Tennant, A. F., & Yukita, M. 2011, *ApJ*, **741**, 49
- Takahara, F. 1979, *PThPh*, **62**, 629
- The Fermi-LAT Collaboration 2019, arXiv:1902.10045
- Tully, R. B. 1988, *Nearby Galaxies Catalog* (Cambridge: Cambridge Univ. Press)
- Ueno, S., Mushotzky, R. F., Koyama, K., et al. 1994, *PASJ*, **46**, L71